



Thermo-Hydraulic Performance Analysis on the Effects of Truncated Twisted Tape Inserts in a Tube Heat Exchanger

Mehdi Ghalambaz ^{1,2}, Ramin Mashayekhi ³, Hossein Arasteh ⁴, Hafiz Muhammad Ali ⁵, Pouyan Talebizadehsardari ^{6,7,*}  and Wahiba Yaïci ^{8,*} 

¹ Institute of Research and Development, Duy Tan University, Da Nang 550000, Vietnam; mehdi.ghalambaz@duytan.edu.vn

² Faculty of Electrical–Electronic Engineering, Duy Tan University, Da Nang 550000, Vietnam

³ Research & Development Team, Couette Limited, Altrincham WA14 2PX, UK; info@couette.co.uk

⁴ Department of Mechanical Engineering, Isfahan University of Technology, Isfahan 8415683111, Iran; h.arasteh@iut.ac.ir

⁵ Mechanical Engineering Department, King Fahd University of Petroleum and Minerals, Dhahran 31261, Saudi Arabia; h.m.ali@qmul.ac.uk

⁶ Metamaterials for Mechanical, Biomechanical and Multiphysical Applications Research Group, Ton Duc Thang University, Ho Chi Minh City 758307, Vietnam

⁷ Faculty of Applied Sciences, Ton Duc Thang University, Ho Chi Minh City 758307, Vietnam

⁸ CanmetENERGY Research Centre, Natural Resources Canada, 1 Haanel Drive, Ottawa, ON K1A 1M1, Canada

* Correspondence: ptsardari@tdtu.edu.vn (P.T.); wahiba.yaici@canada.ca (W.Y.); Tel.: +44-115-837-6859 (P.T.); +1-613-996-3734 (W.Y.)

Received: 10 September 2020; Accepted: 29 September 2020; Published: 9 October 2020



Abstract: This paper investigates the convective heat transfer in a heat exchanger equipped with twisted tape elements to examine effects of the twisted tape truncation percentage, pitch value, position and Reynolds number using 3D numerical simulation. A symmetric heat flux is applied around the tube as the studied heat exchanger. Based on the influences in both heat transfer enhancement and pressure drop, the performance evaluation criterion (PEC) is utilized. Inserting twisted tape elements and reducing the pitch value significantly augment the Nusselt number, friction coefficient and PEC number compared to the plain tube. For the best case with a Reynolds number of 1000, the average Nusselt number increases by almost 151%, which is the case of fully fitted twisted tape at a pitch value of $L/4$. Moreover, increasing the twisted tape truncation percentage reduces both heat transfer and pressure drop. Furthermore, the highest heat transfer rate is achieved when the truncated twisted tape is located at the entrance of the tube. Finally, it is concluded that for $P = L, L/2, L/3$ and $L/4$, the optimum cases from the viewpoint of energy conservation are twisted tapes with truncation percentages of 75, 50, 50 and 0%, in which the related PEC numbers at a Reynolds number of 1000 are almost equal to 1.08, 1.24, 1.4 and 1.76, respectively.

Keywords: truncated twisted tape; secondary flow; laminar convective heat transfer; performance evaluation criterion; CFD; heat exchanger

1. Introduction

Modifying heat transfer is a principal matter of concern for energy conservation and also advantageous from an economic viewpoint. Since heat exchangers are commonly used in almost all areas of industrial activities, including fuel cells [1], electronic device cooling [2], solar air collectors [3], aerospace engineering [4], flame stabilization [5], refrigeration [6], electric vehicles [7], natural gas

liquefaction [8], air dehumidification [9] and so forth, increasing the thermal performance is of vital importance. To satisfy such a need, in the last two decades, researchers have proposed different passive techniques for heat transfer augmentation, including roughness elements [10], twisted tapes [11] and wires inserts [12]. Such equipment modifies heat transfer using a higher heat transfer surface, generating a swirl flow, as well as disturbing hydrodynamic and thermal boundary layers of the fluid inside the tube, which directly improves the heat transfer coefficient.

Among the proposed passive techniques in the literature, applying twisted tape inserts with different geometries in various systems, such as solar collectors [13,14] and solar water heating systems [15–17], has been the focus of attention among experts of the field. Due to large numbers of applications, embedding the twisted tape inserts in double-pipe heat exchangers has recently been studied by many researchers. Man et al. [18] experimentally investigated twisted tape inserts in an inner tube of a double pipe with clockwise and counterclockwise swirling directions. They showed that the heat exchanger thermal performance increases in the presence of twisted tape inserts, presenting a maximum value of 1.42 for the performance evaluation criterion (PEC) number. Lim et al. [19] performed a pitch investigation of twisted tape inserts in a double pipe and reported heat transfer characteristics for different Reynolds number values. Another evaluation of thermal efficiency of a double pipe equipped with twisted tapes using the ε -NTU (Effectiveness—Number of transferred unit) method was performed by Ravi Kumar et al. [20]. They found higher values for both the effectiveness and NTU of the heat exchanger when the twisted tapes were applied. Employing nanofluids [21], hybrid nanofluids [22,23], nano-encapsulated phase change suspensions [24–26] and boiling heat transfer [27,28] are also other promising approaches to improve heat transfer.

Besides, many papers focused on the geometrical aspects of twisted tapes, such as the effects of pitch and width ratios. Jaramillo et al. [29] assessed a parabolic trough collector equipped with twisted tape. They showed that the thermal performance of the collector increased as the twisted ratio reduced at low Reynolds numbers. Mwesigye et al. [30] studied a parabolic trough collector with wall-detached twisted tape. They indicated that higher values of twist ratio and lower values of width resulted in the enhancement of the optimal Reynolds number. Esfe et al. [31] inserted the twisted tapes in a tri-lobbed tube for Reynolds numbers of 5000 to 20,000. Their results revealed that increasing the tape ratio, which is the tape radial length to pipe diameter ratio, enhances the Nusselt number, friction coefficient and overall thermal performance.

Another technique for a higher heat transfer rate using twisted tape is to increase the flow mixing and secondary flow effects by changing the geometry of the twisted tape surface. Saylroy and Eiamsa-ard [32] examined the thermohydraulic performance of a tube equipped with a square-cut twisted tape. These researchers found a maximum PEC value of 1.32 for their captured models in which the thermal performance improved 1.32 times in comparison with the classically twisted tape inserts. In another study [33], they evaluated a multi-channel twisted tape and showed laminar convection heat transfer with twisted tapes embedded in the channel. He et al. [34] examined the thermal behavior of cross hollow, twisted tape inserts in a pipe. They showed PEC values of 0.87–0.98 for Reynolds numbers of 5600–18,000. Samruaisin et al. [35] investigated numerically and experimentally the free space ratio and twisted tape arrangement for regularly spaced quadruple twisted tape inserts in a tube, in a turbulent flow regime. In the range of their operational conditions, they presented a maximum PEC number equal to 1.27. Centrally perforated twisted tape elements in a tube were investigated by Ruengpayungsak et al. [36] for convective heat transfer enhancement under laminar and turbulent flow regimes. Maximum PEC values of 8.92 and 1.33 were reported for laminar and turbulent regimes, respectively. Hasanpour et al. [37] optimized a corrugated tube heat exchanger equipped with twisted tape elements with the purpose of heat transfer modification and pressure drop reduction. They showed that the V-cut twisted tape model causes maximum heat transfer, and the perforated twisted tape model leads to the smallest pressure drop.

Despite using classical twisted tape elements with a gap between the tape and walls, the use of overlapped twisted tapes due to the lower pressure drop penalty was also studied by some researchers. Hong et al. [38] carried out an empirical study of a spiral-grooved tube equipped with twin overlapped twisted tapes in a turbulent regime with Reynolds numbers of 8000 to 22,000. They showed an enhancement in both heat transfer and friction coefficient augmented by the overlapped twisted ratio. In another study [39], they employed overlapped multiple twisted tapes in a similar experimental study. They showed that entropy generation increases and decreases due to friction resistance and heat transfer, respectively, as the tape number changes and overlapped twisted ratio decreases. Eiamsa-Ard and Samravysin [40] carried out an empirical study to investigate the thermal performance of a tube heat exchanger equipped with overlapped quadruple twisted tape inserts compared to typical quadruple twisted tape elements with a Reynolds number ranging from 5000 to 20,000, under a turbulent regime. They reported a maximum value of 1.58 for the PEC number in the case of overlapped quadruple counter tapes in a cross arrangement at a Reynolds number of 5000. Later, overlapped dual twisted tapes, along with Al_2O_3 nanofluid, were studied by Rudrabhiramu et al. [41], with the objective of improving the thermal performance of a heat exchanger. They reported that using 1% nanofluid volume concentration and twisted tape with a twist ratio of two causes the best result.

Some researchers also benefited from compound techniques of heat transfer enhancement using nanofluid along with twisted tape inserts. Qi et al. [42] experimentally investigated the convective nanofluid heat transfer in a tube using rotating and static built-in twisted tape elements. They reported a 101.6% enhancement in heat transfer by using rotating twisted tape inserts along with the nanofluid. In another empirical study, Sunder et al. [43] examined the thermal performance of a solar water heater employing nanofluid and twisted tape inserts as the heat transfer enhancement techniques. They showed a 49.75% improvement using the best configuration of twisted tape.

The above literature review indicates that there are a substantial number of papers using twisted tape inserts in different ways and techniques to reach a model for heat transfer rate maximization and pressure drop minimization. However, reviewing the preceding papers reveals that the hydrothermal investigation of truncated twisted tapes in tubes has not been studied so far. Motivated by this research gap, this study examines the twisted tape truncation percentage and its position in the tube at different pitch values and Reynolds numbers. This paper provides guidelines for the novel usage of twisted tapes in tubes toward higher performance.

2. Problem Statement and Boundary Conditions

Figure 1 schematically shows the tube with twisted tape. The height of the proposed twisted tape (H) is 95% of the tube diameter ($D = 20$ mm) with a thickness (t) of 0.4 mm. Four different twisted tape pitches (P) are investigated, as shown in Figure 1a. To study the position of truncated twisted tape, three different locations, i.e., entrance, center and exit, are examined, as shown in Figure 1b. Note that the length of the tube is 400 mm. Water enters the tube at 300 K with uniform velocity, and a symmetrical constant heat flux of 5000 W/m^2 is applied on the walls, while the twisted tape walls are thermally insulated. A pressure outlet condition is also employed for the tube outlet [44–46].

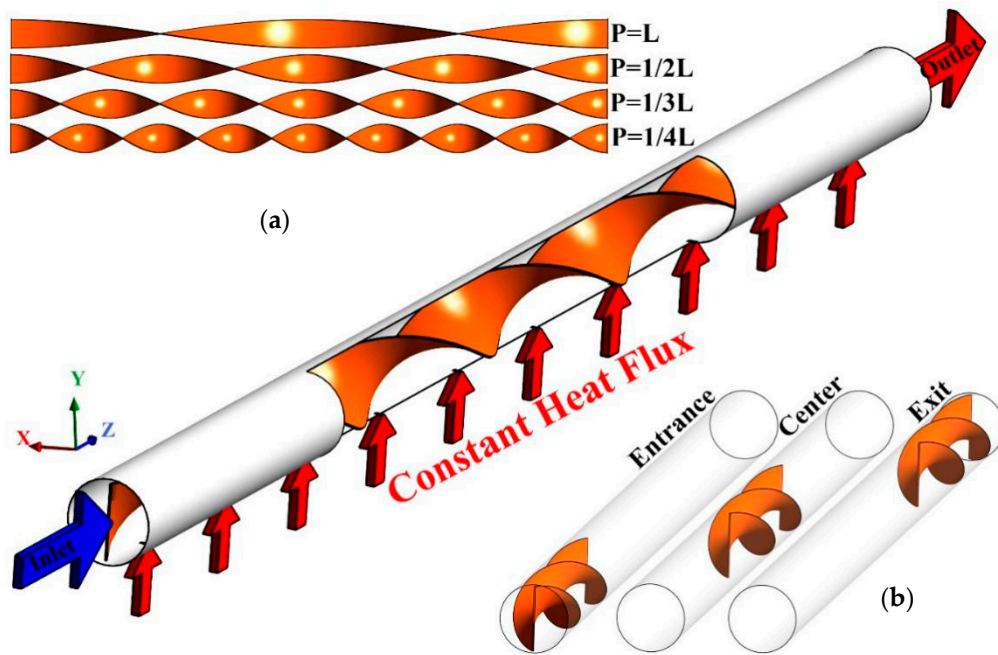


Figure 1. Schematic of the proposed system for (a) different twisted tape pitches and (b) different twisted tape positions.

3. Governing Equations

This research investigates a steady laminar flow of incompressible nanofluid, neglecting the effects of radiation and viscosity losses. The governing equations are defined as follows:

$$\nabla \cdot (\rho \vec{V}) = 0 \quad (1)$$

$$\nabla \cdot (\rho \vec{V} \vec{V}) = -\nabla p + \mu \nabla^2 \vec{V} \quad (2)$$

$$\nabla \cdot (\rho \vec{V} C_p T) = \nabla \cdot (k \nabla T) \quad (3)$$

Different parameters calculated in this study, including the average and local heat transfer coefficient and Nusselt number, friction factor and PEC are defined as follows [36,37]:

$$D_h = \frac{4A}{P} \quad (4)$$

$$f = \frac{2\Delta P D_h}{\rho V^2 L} \quad (5)$$

$$h_x = \frac{q''}{T_w - T_b} \quad (6)$$

$$Nu_x = \frac{h_x D_h}{k} \quad (7)$$

$$Nu_{avg} = \frac{1}{l} \int_0^l Nu_x dx \quad (8)$$

$$PEC = \frac{Nu/Nu_0}{(f/f_0)^{1/3}} \quad (9)$$

4. Numerical Procedure

The commercial ANSYS Fluent computational fluid dynamics (CFD) code is employed to perform the simulation and solve the equations [47–49]. The velocity–pressure coupling is resolved using the coupled algorithm, and the convection terms are discretized using the second-order upwind scheme. The convergence criteria of 10^{-6} are also selected.

4.1. Grid Study

Figure 2 illustrates the computational mesh with finer mesh generated in the near-wall region due to velocity and temperature boundary layers and high gradients of variables. A fully structured mesh is created as shown using ANSYS meshing to have a high degree of quality and faster convergence in CFD FLUENT code, which also results in less computational time.

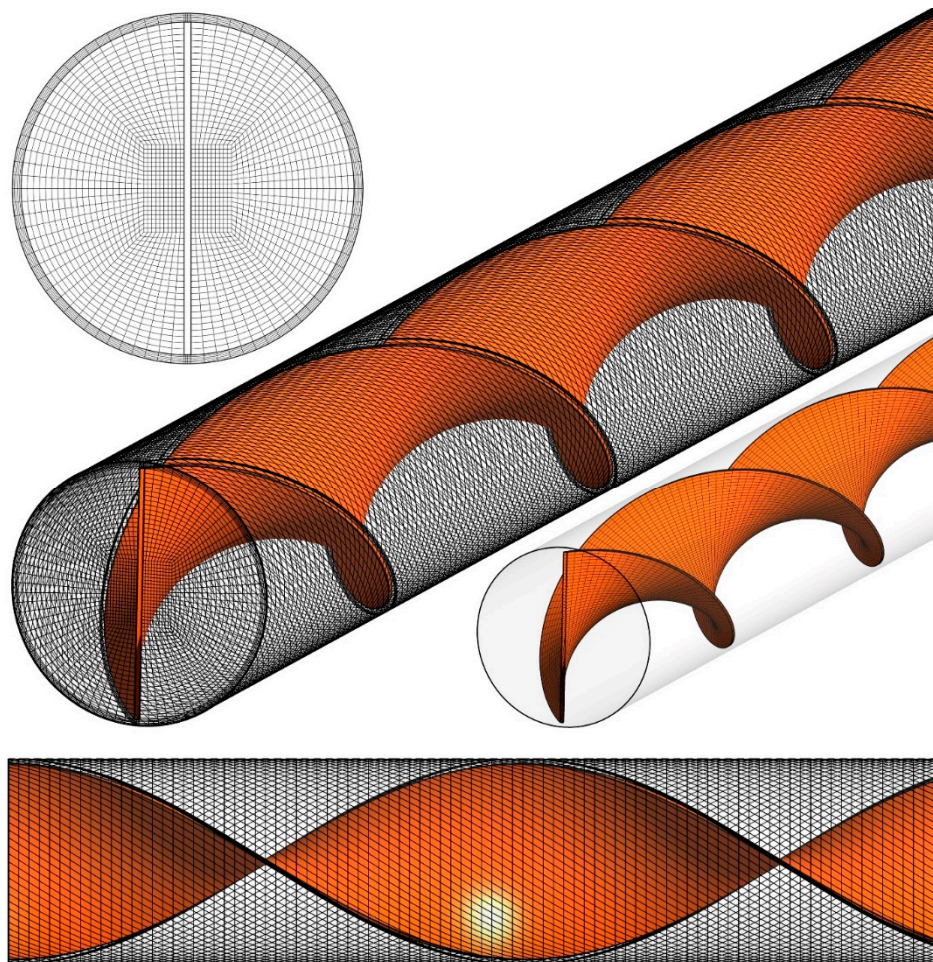


Figure 2. The meshing of the computational domain.

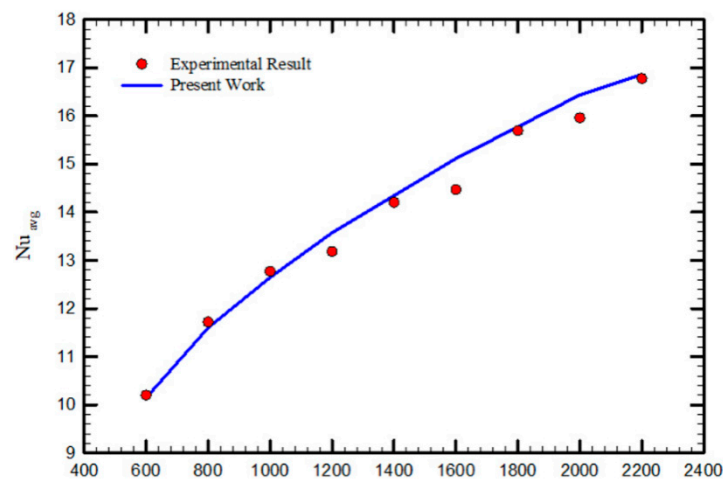
Different grid numbers are examined for grid independency analysis in the case of fully filled twisted tape with a pitch of $L/4$ and a Reynolds number of 1000. The average Nusselt number is selected as the selection criterion [50] presented in Table 1. As listed, case 3 is chosen for all the simulations, since using finer meshing leads to relative errors of less than one percent.

Table 1. Grid independence analysis.

Case	Number of Elements	Nusselt Number	Error (%)
1	750,000	41.61	-
2	1,250,000	39.12	5.98
3	1,750,000	38.04	2.74
4	2,250,000	37.85	0.52
5	3,000,000	37.7	0.39

4.2. Validation

To obtain a reliable result, the experimental results of Qi et al. [42] for the average Nusselt number for laminar fluid flow in a heat exchanger using stationary twisted tape are used. They experimentally examined pure water and nanofluid flow for different Reynolds numbers for a twisted tape length of 1600 mm and a pitch size of 100 mm with a width and thickness of 16 and 2 mm, respectively. Figure 3 displays the average Nusselt number for the cases of pure water and stationary twisted tapes for different Reynolds numbers. As shown, the results are in excellent agreement with the experimental data of Qi et al. [42], where the maximum difference is less than 2%.

**Figure 3.** Validation of the present numerical results with the experimental data of Qi et al. [42].

5. Results and Discussion

Numerical simulations are performed at four pitch values (P) of L , $L/2$, $L/3$ and $L/4$, four Reynolds numbers (Re) of 250, 500, 750 and 1000, three twisted tape truncation (λ) percentages of 25, 50 and 75% and three positions of twisted tape at the entrance, center and exit of the tube, which are investigated in the following:

5.1. Effect of Twisted Tape Pitch

In the first step, the effect of twisted tape pitch on the hydrothermal characteristics of the tube is examined and analyzed. Figure 4 represents the local Nusselt number (Nu) throughout the tube length for the plain tube (PT) and four twisted tape pitch values at $Re = 250$ while the twisted tape is fully fitted in the tube (no truncation). Using the twisted tape and decreasing its pitch magnitude noticeably augments the local Nu along the tube length. The reason is that the twisted tape inserts create secondary flow as a result of flow swirling, which consequently improves the flow mixing, disturbs the thermal boundary layer and increases the heat transfer rate [51]. In other words, the twisted tape redirects the colder core fluid with a better cooling capacity to the heated walls of the tube where cooling is required.

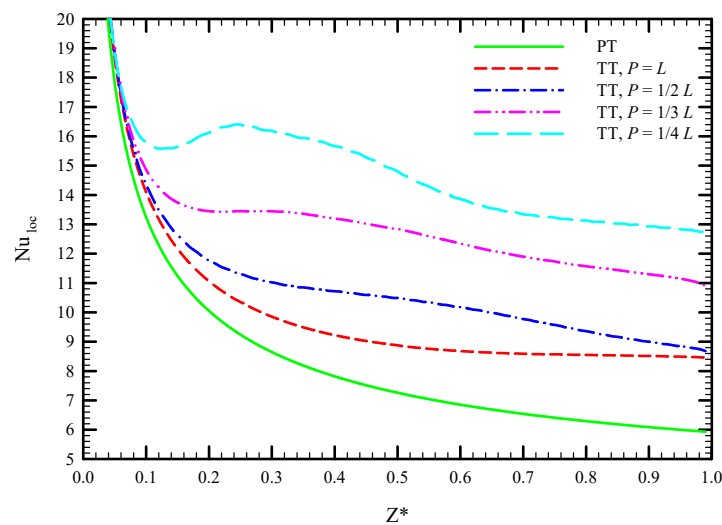


Figure 4. Local Nu along the tube length for plain tube (PT) and twisted tape inserts with $P = L, L/2, L/3, L/4$ at $Re = 250$.

The cause of the heat transfer enhancement in Figure 4 can be seen in Figure 5, in which the streamlines colored by velocity magnitude are illustrated for PT and four twisted tape pitch values. It is visible that as the twisted tape pitch value decreases, the flow path undergoes more changes. This is because more swirl flow fronts can be seen in lower pitch values with higher radial velocity, implying stronger secondary and mixing flow. As a result, it leads to a more effective redirection of core colder fluid towards the heated wall and, consequently, more heat is transferred between the fluid and heated wall.

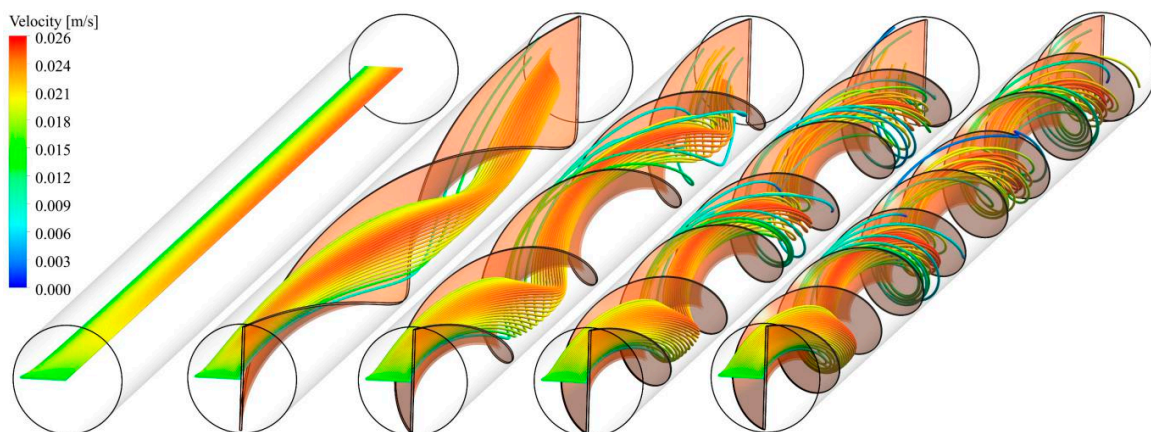


Figure 5. Streamlines colored by velocity magnitude for PT and twisted tape inserts with $P = L, L/2, L/3, L/4$ at $Re = 250$.

Figure 6 shows how decreasing the twisted tape pitch magnitude affects the cooling of the heated wall at $Re = 250$. The temperature distribution on the heated wall implies that the secondary and mixing flow intensity affect the heated wall. In PT, the uniform enhancement of temperature along the tube length is visible, showing the thermal boundary layer development without any disturbance. On the contrary, as the twisted tape is inserted in the tube, the change in temperature distribution on the heated wall is visible. The temperature value on the heated wall decreases along the tube length and strengthens as the pitch value reduces. In higher pitch values, some hotspot regions are visible on the heated wall temperature contour; however, these regions decline at lower pitch values, resulting in better cooling performance of the system.

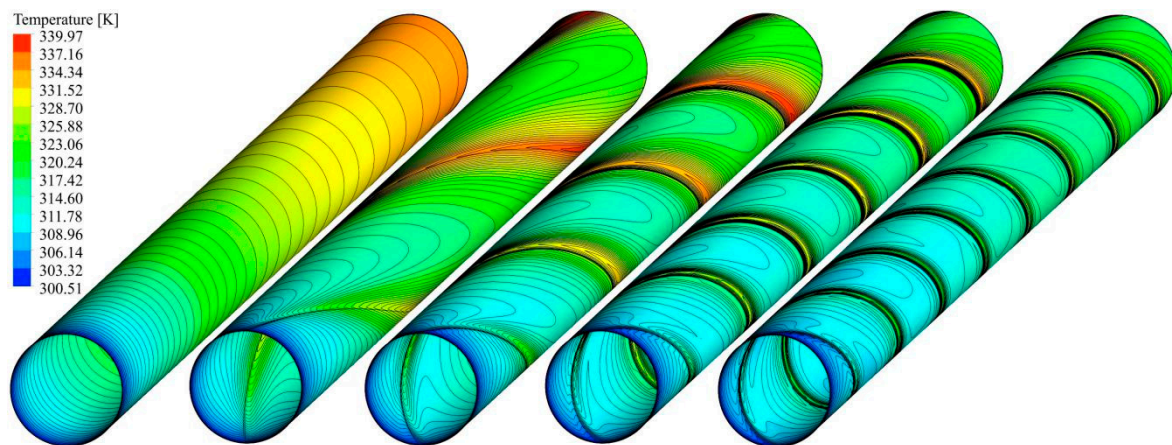


Figure 6. Temperature contours on the heated wall for PT and twisted tape inserts with $P = L, L/2, L/3, L/4$ at $Re = 250$.

To better understand the temperature distribution, four different cross-sections are defined along the tube length and are displayed in Figure 7. In the following, different parameters, such as temperature and velocity, are illustrated in them.

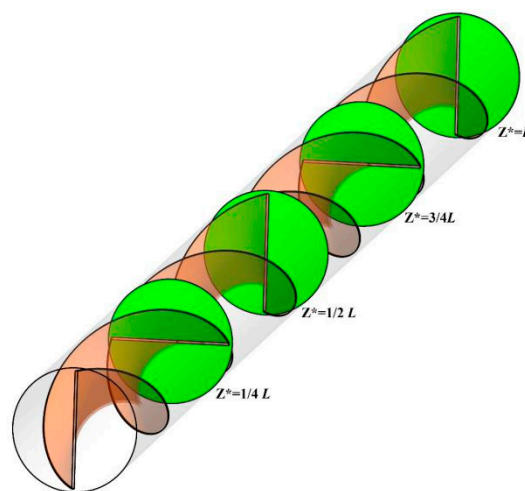


Figure 7. Generated cross-sectional surfaces throughout the tube length for post-processing purposes.

Figure 8 demonstrates the cross-sectional temperature contours on the surfaces shown in Figure 7 for PT and four twisted tape pitch values at $Re = 250$. The PT temperature contours show the normal development of the thermal boundary layer throughout the tube, leading to a great drop in heat transfer along the tube. On the other hand, the thermal boundary layer disturbance is intensified and gets thinner as the twisted tape is inserted in the tube, which is more effective for a lower pitch in heat transfer between the fluid and heated wall. Besides, fewer hotspot regions causing a reduction in heat transfer enhancement is visible at lower pitch values of the twisted tape, proving the cooling process improvement. Another point that can be noticed in this figure is that the presence of twisted tape and lowering its pitch value redirects the core colder fluid to the vicinity of the hot wall. The twisted tape causes more efficient heat dissipation from the wall and, consequently, more heat is transferred from the wall to the fluid. It should be noted that the contours are almost symmetrical, related to the center of the tube in all cases.

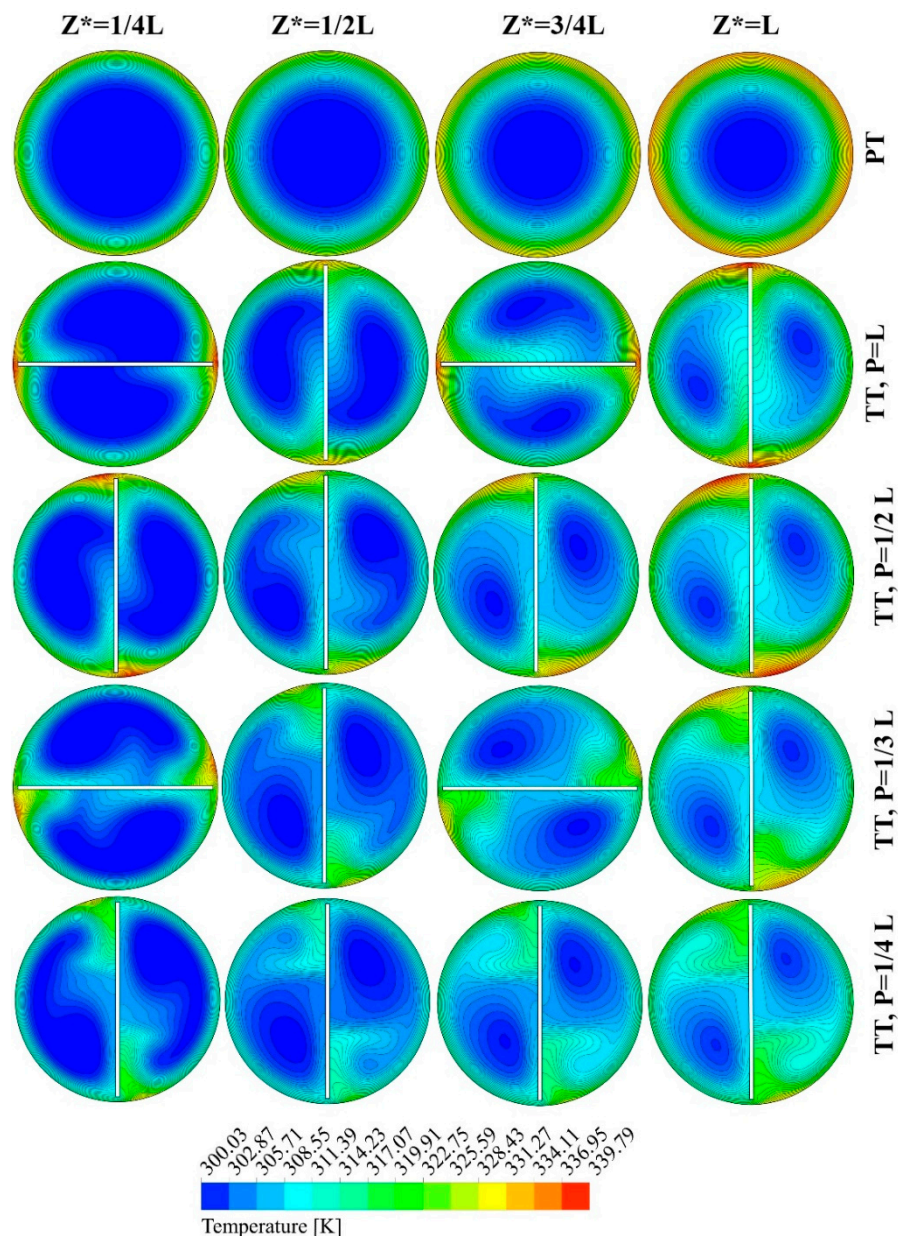


Figure 8. Cross-sectional temperature contours for PT and twisted tape inserts with $P = L, L/2, L/3, L/4$ at $Re = 250$.

Figure 9 displays the cross-sectional velocity contours on the surfaces shown in Figure 7 for PT and four twisted tape pitch values at $Re = 250$. The velocity contours imply the intensity of secondary and mixing flow in the presence of twisted tape inserts. In other words, the higher velocity of the fluid near the heated wall shows a stronger secondary flow, and, as a result, a higher fluid momentum near the wall and a better cooling process could be achieved. It is visible in this figure that inserting twisted tape with a pitch value of L results in a high-velocity region of the fluid, which is strengthened as the twisted tape pitch value decreases, resulting in the stronger secondary flow observed in Figure 5. It should be noted that the contours are almost symmetrical, related to the center of the tube in all cases; however, for the case with $P = L$, it is almost symmetrical related to the twisted tape plane.

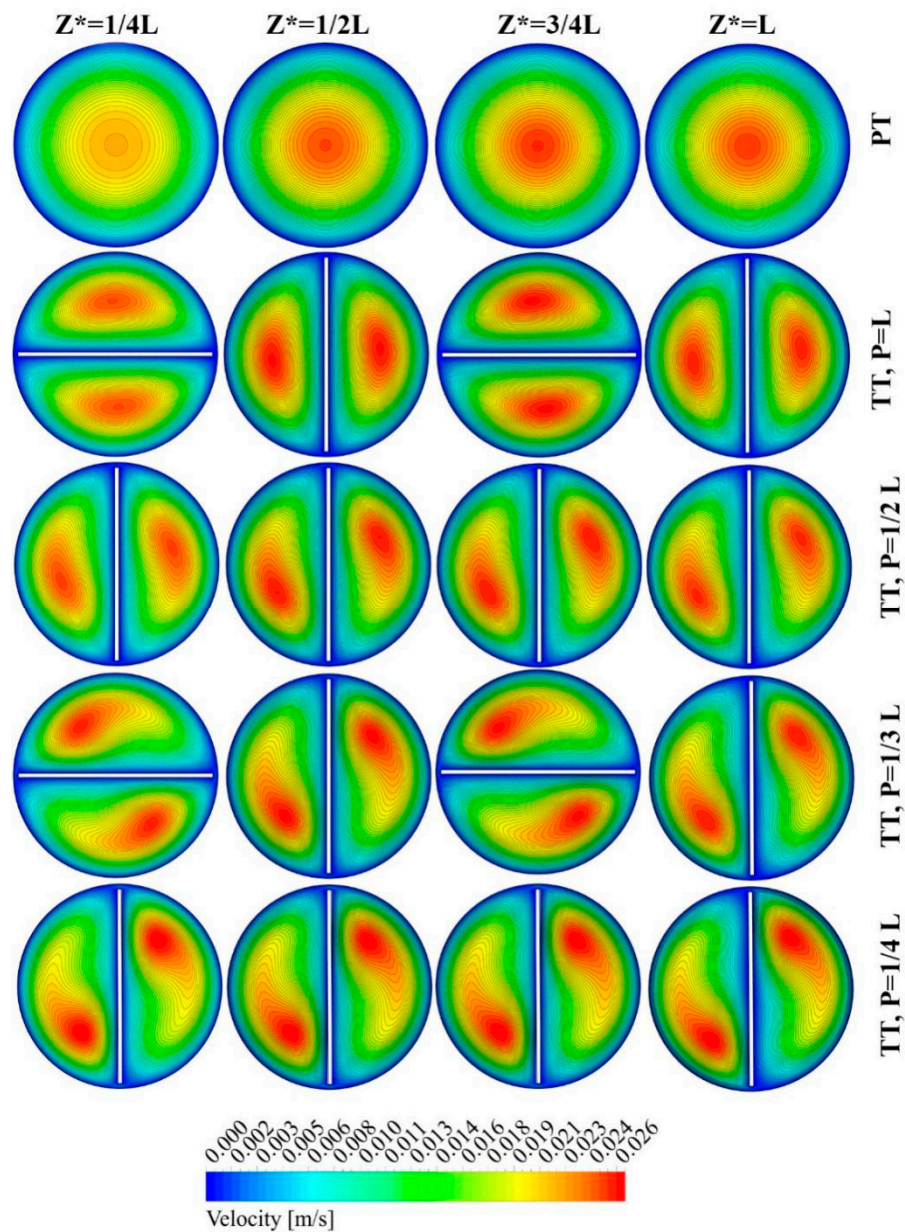


Figure 9. Cross-sectional velocity contours for PT and twisted tape inserts with $P = L, L/2, L/3, L/4$ at $Re = 250$.

To better quantify the heat transfer modification in the presence of twisted tape inserts with different pitch values, Figure 10 is provided for various Re . Nu increases as Re changes due to the more effective advection phenomenon and fluid momentum in higher fluid velocities. As seen in this figure, as an example, using twisted tape with pitch values of $L, L/2, L/3$ and $L/4$ increases the average Nu by about 26.87, 55.03, 86.59 and 151.42% at $Re = 1000$ compared with the PT, respectively.

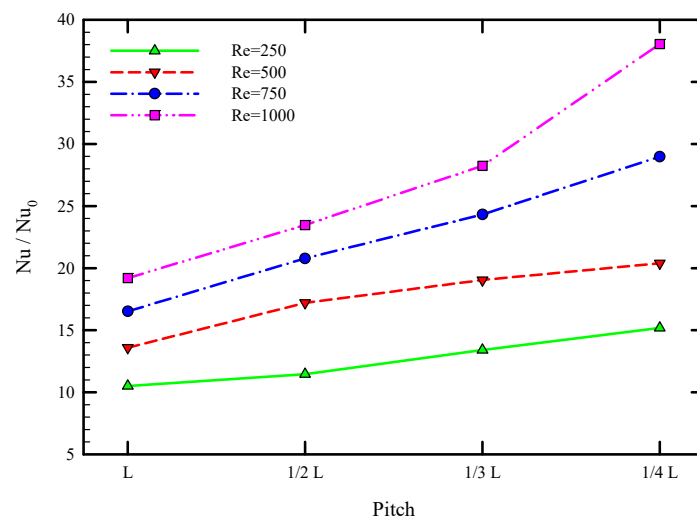


Figure 10. Variations of average Nu ratio with respect to PT at various pitch values and Re .

Figure 11 shows the variations of the friction coefficient ratio with respect to PT for different pitch values and Re . This figure shows that applying twisted tape enhances the friction coefficient ratio due to the added surface area and flow blockage [52]. Furthermore, higher values for the friction coefficient ratio are observed in lower pitch values due to the creation of the more intense secondary flow shown in Figure 5; however, when the twisted tape pitch is equal to L , its enhancement is insignificant due to the creation of very weak secondary flow in the tube. Moreover, this figure reveals that the friction coefficient ratio increases as Re changes because more intense swirling flow.

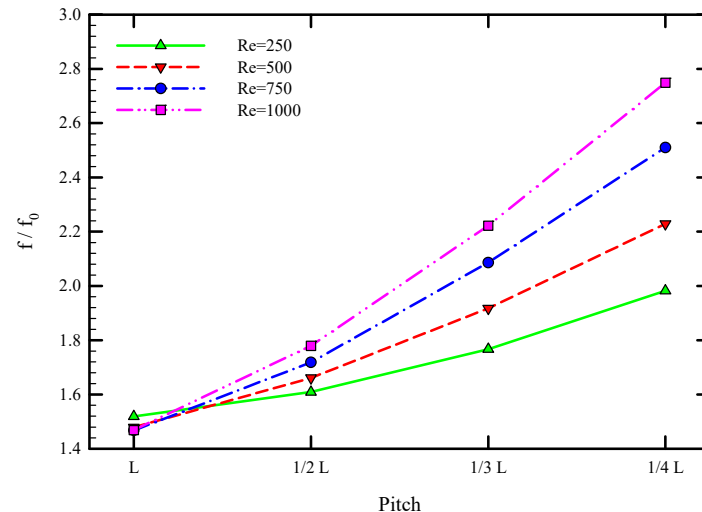


Figure 11. Variations of friction coefficient ratio with respect to PT at various pitch values and Re .

5.2. Effect of Truncated Twisted Tape Position and Percentage

So far, it has been shown that the twisted tape with a pitch of $L/4$ results in the best thermal performance of the system. Therefore, the following simulations are performed for this pitch value. To show the effect of twisted tape truncation percentage on local Nu throughout the tube length for different twisted tape positions, Figure 12 is provided at $Re = 250$. In Figure 12a, the twisted tape is embedded at the entrance of the tube with different values for λ . It is visible that as the flow enters the twisted tape at the tube inlet, the thermal boundary layer is disturbed and, due to the creation of secondary flow, the local Nu increases; however, as the flow passes the twisted tape, the thermal boundary layer starts to develop normally, and as a result, it tends to develop towards the local Nu

curve of PT. Consequently, lower values of λ cause a higher heat transfer rate when the twisted tape is inserted at the tube entrance.

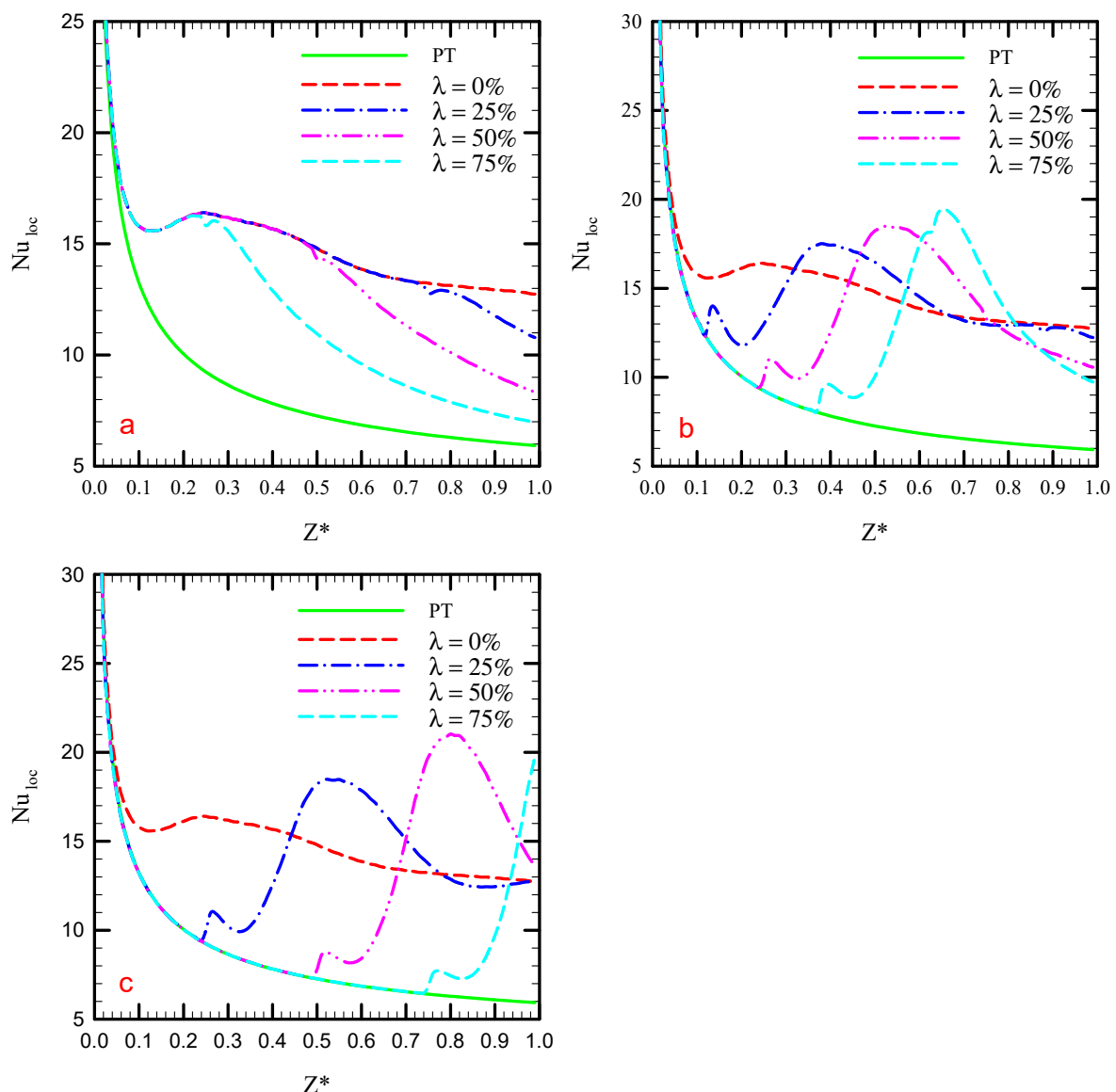


Figure 12. Local Nu along the tube length for different λ values at three twisted tape positions for (a) entrance, (b) center, (c) exit and $P = L/4$.

In Figure 12b, the twisted tape is embedded at the center of the tube with different values for λ . In this figure, the local Nu curve starts to grow as the fluid reaches the twisted tape due to the thermal boundary layer disturbance. It is visible that the local Nu at the truncated cases surpasses the fully fitted twisted tape, and a higher maximum value for Nu is visible for higher values of λ . As the flow passes the twisted tape, the thermal boundary layer starts to grow and becomes fully developed.

In Figure 12c, the twisted tape is embedded at the exit of the tube with different values for λ . This figure also shows the local Nu enhancement as the fluid enters the twisted tape as a result of thermal boundary layer disturbance and stronger mixing flow. In this case, after a sudden increase in Nu at the twisted tape entrance, the local Nu decreases, and its curve tends to reach the value of the fully fitted twisted tape.

Figure 13 displays the streamlines colored by velocity magnitude in different twisted tape truncation percentage values inserted at the tube entrance for $Re = 250$. In the truncated cases, the flow

path swirls to the end of tube length, but the secondary flow intensity is reduced as the fluid passes the twisted tape. As a result, truncating the twisted tape results in a reduction in heat transfer rate but less material is used, causing fewer production expenses, and also the pressure loss penalty reduces due to less flow lockage and contact area between the fluid and solid.

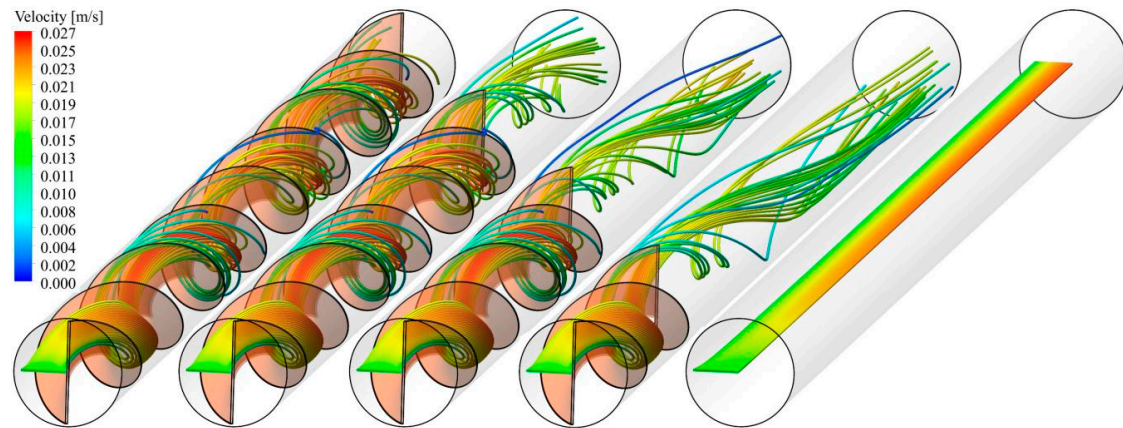


Figure 13. Streamline colored by velocity magnitude for different λ values at $Re = 250$ and $P = L/4$.

To show the effect of truncated twisted tape inserts and changes in the flow patch shown in Figure 13 on the temperature distribution of the heated wall, Figure 14 illustrates the temperature contours at the wall. It is visible that although there are some hotspots after the truncated twisted tape, the number of hotspots is still lower than for the PT, showing the effective cooling process even after the fluid passes the twisted tape. This figure proves the presence of secondary flow (not as intense as it is in the fully twisted tape insert) after the fluid passes the truncated twisted tape.

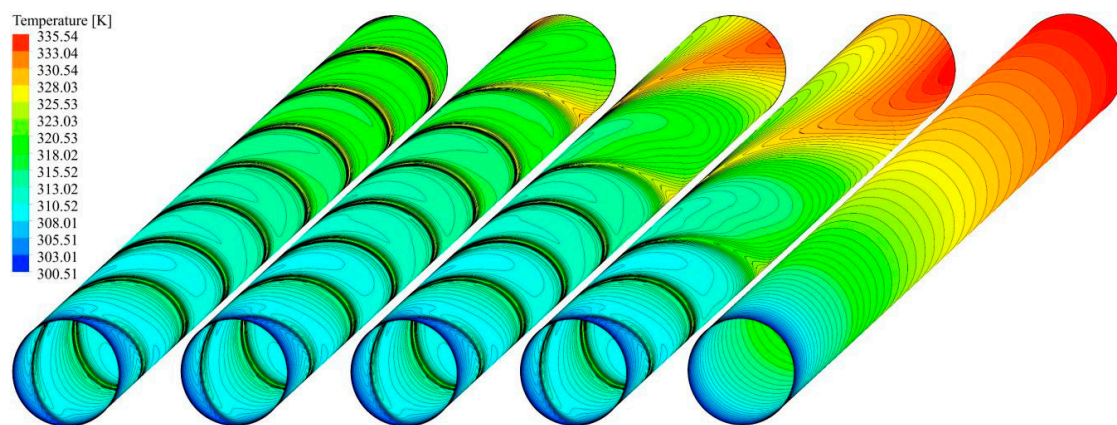


Figure 14. Temperature contours on the heated wall for different λ values at $Re = 250$ and $P = L/4$.

To clearly show the effect of twisted tape position on the local Nu throughout the tube length at different twisted tape truncation percentage values, Figure 15 illustrates the local Nu for three different twisted tape truncation percentage values of 25, 50 and 75% at $Re = 250$ for different positions, as shown in Figure 1b. This figure shows that when the twisted tape is at the tube entrance, no sudden increase in Nu is visible; in contrast, there is a maximum value for Nu along the tube length when the twisted tape is inserted at the center and exit of the tube. For all values of λ , the highest maximum Nu throughout the tube length corresponds to the layouts where twisted tape is inserted at the tube exit, which is higher as λ changes.

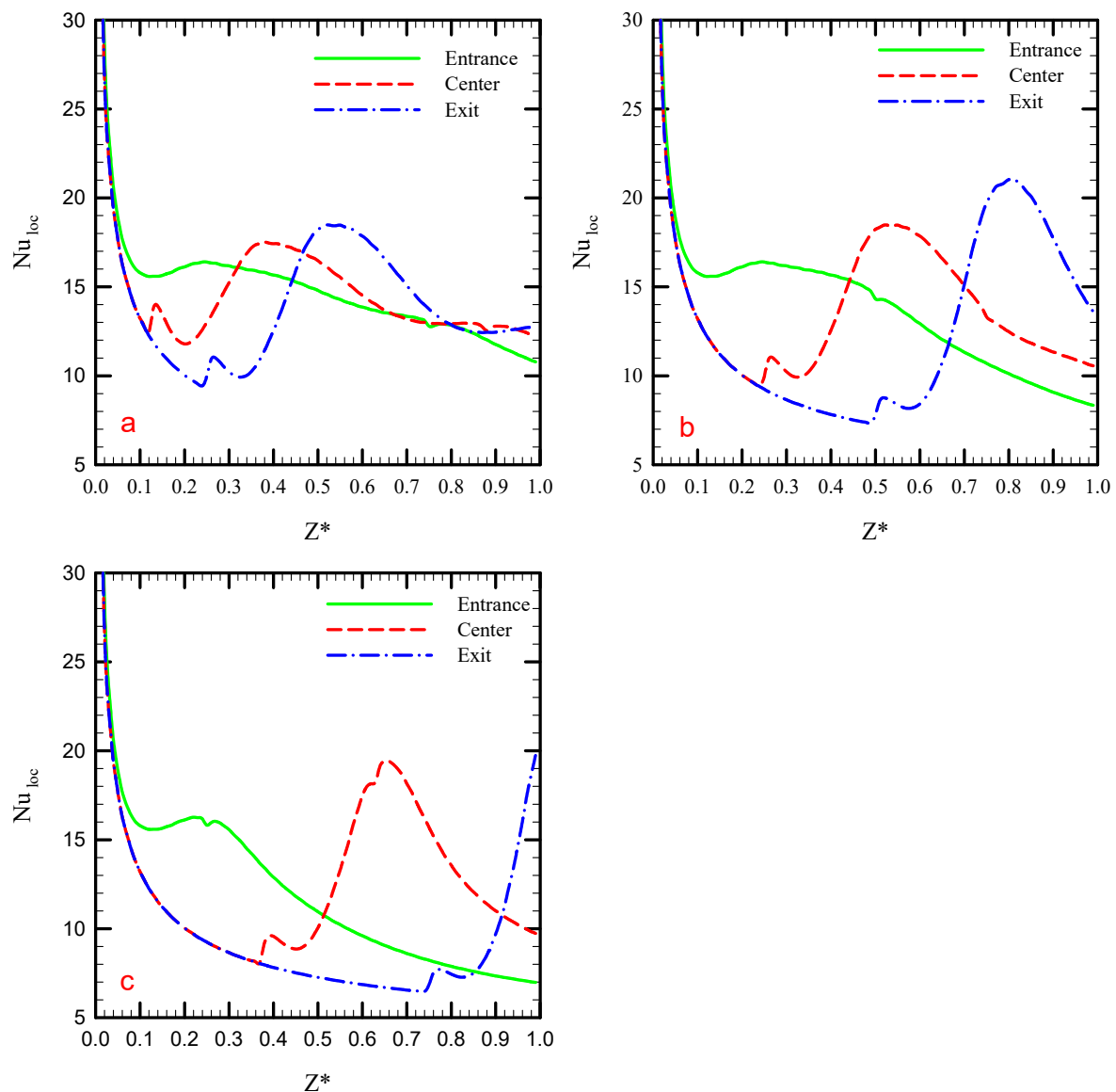


Figure 15. Local Nu along the tube length for different twisted tape positions at three λ values of (a) 25%, (b) 50%, (c) 75% and $P = L/4$.

Figure 16 illustrates the streamlines colored by velocity magnitude at different positions of the twisted tape in the tube at a twisted tape truncation percentage of 75% and $Re = 250$. This figure shows that when the twisted tape is embedded at the tube entrance, the whole flow patch is affected. When the twisted tape is at the tube center, half of the tube length is affected, and for the case in which twisted tape is at the tube exit, the flow path before reaching the twisted tape is similar to that of PT.

The effect of the position of the truncated twisted tape inserts on the temperature distribution of the heated wall is depicted in Figure 17. The same temperature distribution before the flow reaches the twisted tape as that of PT for the heated wall temperature distribution is also visible in this figure. Moreover, flow mixing as the fluid passes the twisted tape and the strong secondary flow in the twisted tape regions are observable in this figure.

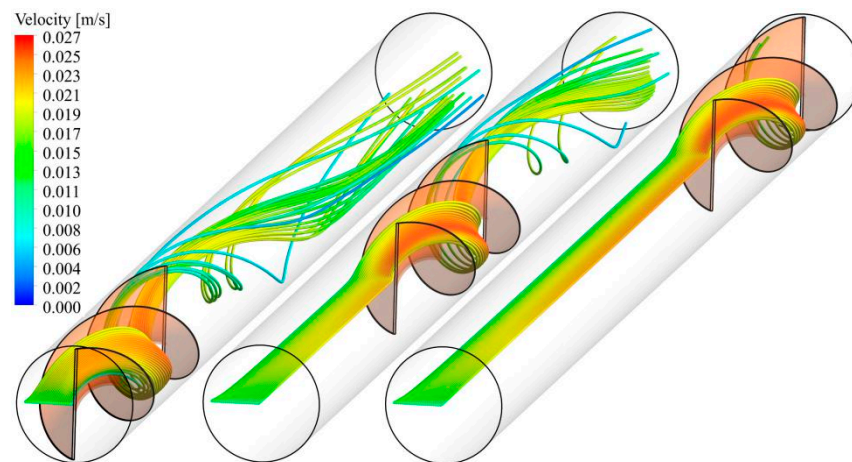


Figure 16. Streamline colored by velocity magnitude for different twisted tape positions at $Re = 250$, $P = L/4$ and $\lambda = 0.75$.

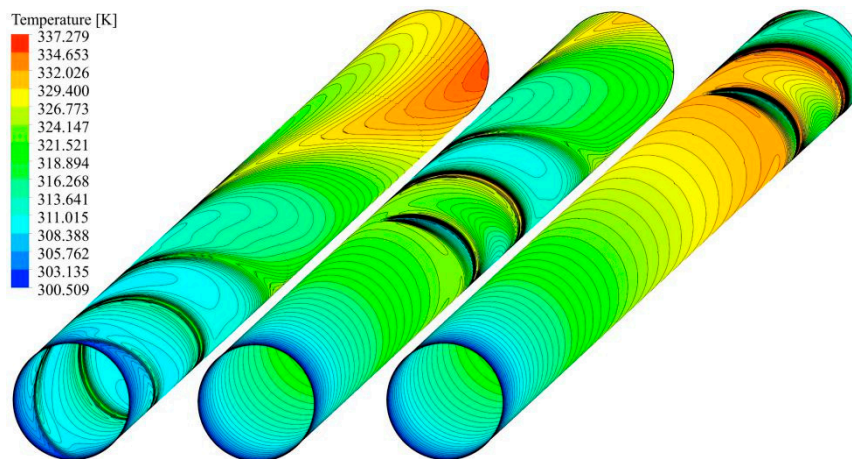


Figure 17. Temperature contours on the heated wall for different twisted tape positions at $Re = 250$, $P = L/4$ and $\lambda = 0.75$.

To quantify the heat transfer rate for different truncation values and positions of the twisted tape, Figure 18 is provided to show the variations of the Nu ratio compared with PT at various λ and Re values, different twisted tape positions and a pitch of $L/4$. For all twisted tape positions and Re , higher values of λ result in lower Nu and heat transfer due to the fact that the secondary and mixing flows in a tube fully fitted with twisted tape are much stronger than for a tube equipped with a truncated twisted tape, as shown in Figure 14. As seen in this figure, using twisted tape with a pitch value of $L/4$ at the entrance of the tube and λ values of 0, 25, 50 and 75% increase the average Nu by about 71.26, 68.50, 57.59 and 37.34% at $Re = 250$ and 151.42, 133.99, 109.52 and 71.43% at $Re = 1000$ in comparison with the PT, respectively.

Considering the position of the twisted tape, for all values of λ at Re of 1000, when the truncated twisted tape is placed at the tube entrance, a higher Nu is obtained, followed by the cases with twisted tape at the tube center, and the lowest Nu correspond to the cases with twisted tape at the tube exit. This is due to the fact that as the fluid passes the twisted tape, the flow is still affected by the twisted tape and swirl flow is visible to the end of the tube, as shown in Figure 16. Thus, for the case of twisted tape inserts in the tube entrance, more of the tube length experiences swirl flow, and as a result, the cooling process improves.

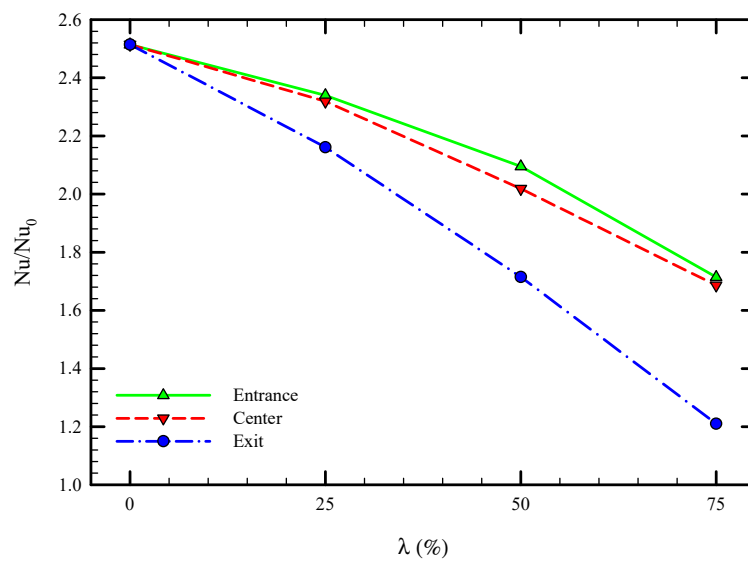


Figure 18. Variations of average Nu ratio with respect to PT at different twisted tape positions and λ values for $Re = 1000$.

Figure 19 represents the variations of friction coefficient ratio with respect to PT at various λ for Re of 1000, different twisted tape positions and a pitch of $L/4$. It is visible that for all twisted tape positions, as λ increases, the friction coefficient ratio is reduced due to the lower level of solid material and, as a result, less flow blockage and smaller contact area between the fluid flow and solid. Furthermore, for all values of λ , there are almost similar values for the friction coefficient ratio for the cases where twisted tape is placed at the tube entrance and center; however, lower values for the friction coefficient ratio are observable when the twisted tape is embedded at the tube exit. The cause of this scenario can be attributed to the fact that when the twisted tape is at the tube exit, no swirl flow is generated before the fluid reaches the twisted tape.

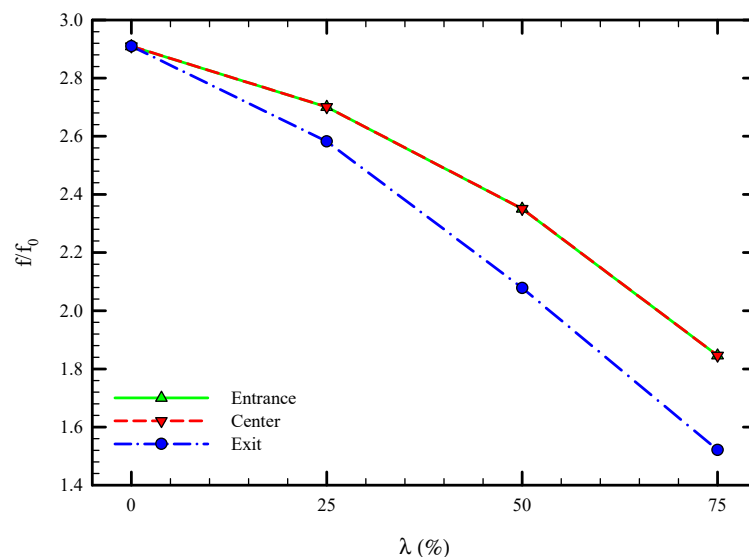


Figure 19. Variations of friction coefficient ratio with respect to PT at different twisted tape positions and λ values for $Re = 1000$.

As discussed above, the application of twisted tape inserts in the captured cases increases both the heat transfer rate as a desirable outcome and the friction coefficient as an undesirable result. Therefore, there is an interplay between the benefits of using twisted tape in heat transfer enhancement and their side effects in forcing more pumping power into the system. To analyze this issue, the dimensionless PEC number introduced in Equation (9) is discussed here. In fact, this number is used to evaluate the practical use of any modified heat transfer technique from the viewpoint of energy-saving potential. Generally, higher values of PEC imply superior energy saving. Figure 20 illustrates the PEC parameter for all cases investigated in this study for Re of 1000. It is visible that decreasing the twisted tape pitch value from Figure 20a–d enhances the PEC number, showing the fact that applying twisted tape with a lower pitch value is efficient from the viewpoint of both heat transfer enhancement and energy saving. It is also visible that as the twisted tape pitch increases, the sensitivity of PEC to the λ value is reduced.

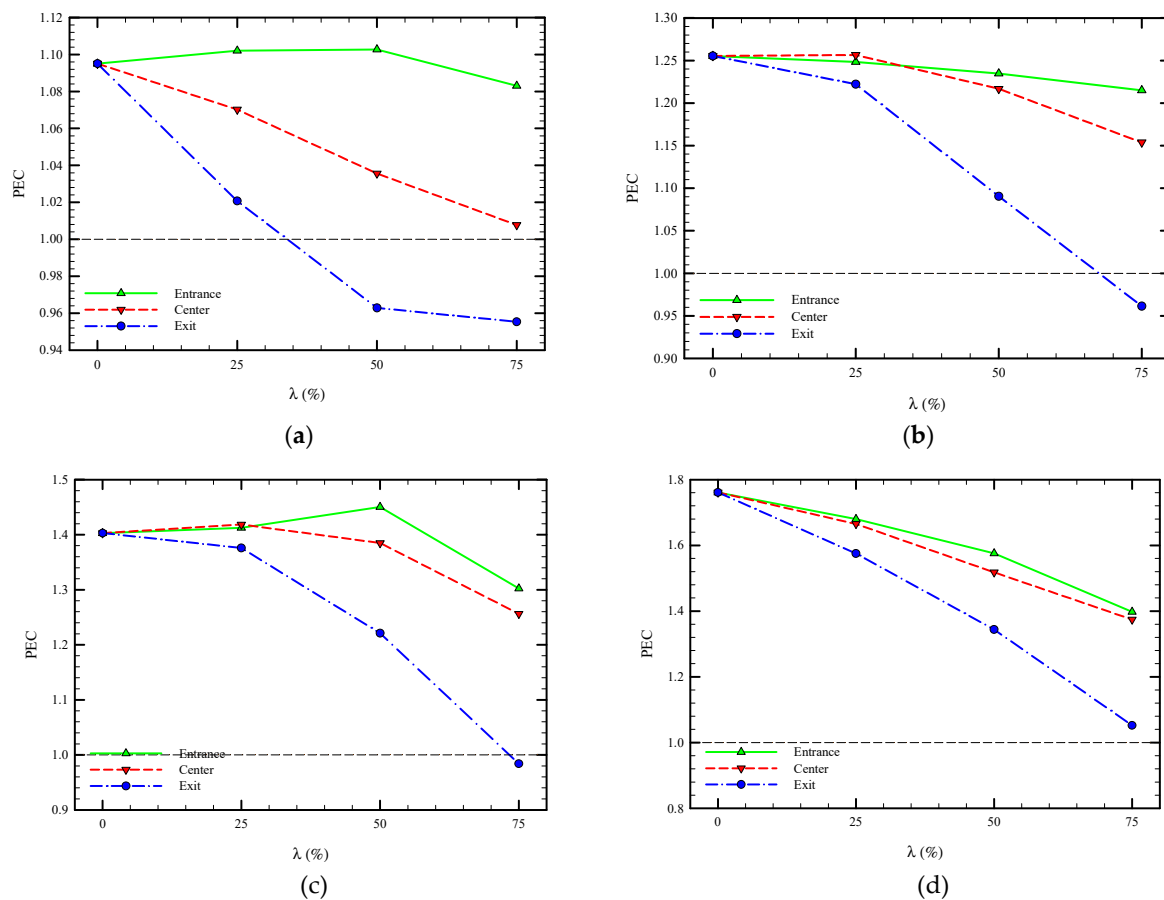


Figure 20. Variations of PEC number at different twisted tape positions, λ and P values. (a) $P = L$, (b) $P = L/2$, (c) $P = L/3$ and (d) $P = L/4$ for $Re = 1000$.

Furthermore, for all λ values, placing the twisted tape at the tube entrance leads to higher PEC magnitudes. Therefore, for $P = L, L/2, L/3$ and $L/4$, the optimum cases from the viewpoint of energy saving are twisted tapes with $\lambda = 75, 50, 50$ and 0% , for which the related PEC numbers at $Re = 1000$ are almost equal to 1.08, 1.24, 1.4 and 1.76, respectively. In addition, PEC numbers in all cases are tabulated in Appendix A of this paper.

6. Conclusions

This paper investigated the laminar convection heat transfer in a tube equipped with twisted tape inserts. A parametric study was conducted to evaluate the impact of key design variables, including the twisted tape truncation percentage, pitch value, position in the tube and Reynolds number on the fluid flow and heat transfer characteristics of such a configuration using symmetric heat flux around the tube. To determine the trade-off between the heat transfer enhancement and the pressure drop penalty, the PEC number was calculated. The obtained results indicated that using the twisted tape and reducing its pitch value increases the Nusselt number, friction coefficient and PEC number due to the generation of efficient secondary and mixing flow. The average Nusselt number increased by about 151.42 for a Reynolds number of 1000 in the case of fully fitted twisted tape at a pitch value of $L/4$. It was also found that increasing the twisted tape truncation percentage reduced both heat transfer and pressure drop in comparison with the fully fitted twisted tape case. Moreover, the best position for the truncated twisted tapes was at the tube entrance to reach the highest thermal performance. Ultimately, it was concluded that for $P = L, L/2, L/3$ and $L/4$, the optimum cases from the viewpoint of energy saving are twisted tapes with $\lambda = 75, 50, 50$ and 0% , for which the related PEC numbers at a Reynolds number of 1000 are almost equal to 1.08, 1.24, 1.4 and 1.76, respectively. The finding of this research provides a framework for researchers working in this area toward higher performance based on energy saving according to both heat transfer enhancement and pressure drop reduction.

Author Contributions: R.M. and P.T. performed and designed the numerical simulations; M.G., H.A., R.M., H.M.A. and W.Y. analyzed the data and performed the discussion; M.G., H.A., R.M., P.T., H.M.A. and W.Y. wrote the paper. All authors have read and agreed to the published version of the manuscript.

Funding: The APC was funded by Dr Wahiba Yaïci from CanmetENERGY Research Centre, Natural Resources Canada.

Conflicts of Interest: The authors declare no conflict of interest.

Appendix A

Table A1. PEC in all cases for twisted tape at the entrance.

λ (%) \ Re	250	500	750	1000	
0	1.011295	1.021043	1.059828	1.095052	P = L
25	1.01388	1.017496	1.045332	1.070205	
50	1.004123	1.006426	1.02249	1.035571	
75	0.995671	0.99766	1.003663	1.007723	
0	1.082103	1.24311	1.265074	1.255414	P = L/2
25	1.089229	1.232876	1.263873	1.256518	
50	1.092546	1.194338	1.220967	1.216784	
75	1.074308	1.131182	1.149658	1.153739	
0	1.227265	1.311893	1.387978	1.402961	P = L/3
25	1.227311	1.319265	1.401682	1.418449	
50	1.210159	1.302567	1.334738	1.384967	
75	1.199981	1.258698	1.265143	1.25622	
0	1.337716	1.336512	1.555087	1.761103	P = L/4
25	1.338476	1.40221	1.515203	1.665051	
50	1.315334	1.37707	1.476264	1.517847	
75	1.29284	1.345982	1.368546	1.374241	

Table A2. PEC in all cases for twisted tape at the center.

λ (%) \ Re	250	500	750	1000	
0	1.011295	1.021043	1.059828	1.095052	P = L
25	1.030648	1.043332	1.079246	1.102066	
50	1.033091	1.058554	1.08903	1.102768	
75	1.018142	1.046153	1.071832	1.083035	
0	1.082103	1.24311	1.265074	1.255414	P = L/2
25	1.109637	1.255035	1.268496	1.248454	
50	1.130221	1.236448	1.245266	1.234765	
75	1.098127	1.18203	1.205088	1.215016	
0	1.227265	1.311893	1.387978	1.402961	P = L/3
25	1.257101	1.318361	1.391219	1.412675	
50	1.246763	1.292509	1.340597	1.450322	
75	1.18302	1.256449	1.293239	1.302188	
0	1.337716	1.336512	1.555087	1.761103	P = L/4
25	1.357279	1.340645	1.49818	1.680165	
50	1.332735	1.385675	1.507737	1.575765	
75	1.237176	1.333577	1.375402	1.397482	

Table A3. PEC in all cases for twisted tape at the exit.

λ (%) \ Re	250	500	750	1000	
0	1.011295	1.021043	1.059828	1.095052	P = L
25	0.984648	0.983887	1.002881	1.02074	
50	0.95755	0.953732	0.958557	0.962848	
75	0.956485	0.954873	0.955329	0.955342	
0	1.082103	1.24311	1.265074	1.255414	P = L/2
25	1.06148	1.185216	1.225127	1.222088	
50	1.005875	1.052004	1.083942	1.090425	
75	0.959385	0.95912	0.960504	0.961318	
0	1.227265	1.311893	1.387978	1.402961	P = L/3
25	1.18397	1.29666	1.343979	1.375853	
50	1.115867	1.214709	1.214682	1.220923	
75	0.971801	0.980115	0.98335	0.98392	
0	1.337716	1.336512	1.555087	1.761103	P = L/4
25	1.294428	1.382539	1.469811	1.574971	
50	1.252857	1.297774	1.344916	1.343726	
75	1.021773	1.049235	1.050204	1.052115	

References

- Hosseini, M.; Afrouzi, H.H.; Arasteh, H.; Toghraie, D. Energy analysis of a proton exchange membrane fuel cell (PEMFC) with an open-ended anode using agglomerate model: A CFD study. *Energy* **2019**, *188*, 116090. [CrossRef]
- Purusothaman, A. Investigation of natural convection heat transfer performance of the QFN-PCB electronic module by using nanofluid for power electronics cooling applications. *Adv. Powder Technol.* **2018**, *29*, 996–1004. [CrossRef]
- Dabiri, S.; Khodabandeh, E.; Poorfar, A.K.; Mashayekhi, R.; Toghraie, D.; Zade, S.A.A. Parametric investigation of thermal characteristic in trapezoidal cavity receiver for a linear Fresnel solar collector concentrator. *Energy* **2018**, *153*, 17–26. [CrossRef]

4. Sakanova, A.; Tong, C.F.; Tseng, K.J.; Simanjorang, R.; Gupta, A.K. Weight consideration of liquid metal cooling technology for power electronics converter in future aircraft. In Proceedings of the 2016 IEEE 2nd Annual Southern Power Electronics Conference (SPEC), Auckland, New Zealand, 5–8 December 2017; pp. 1–5.
5. Ravi, R.; Pachamuthu, S.; Kasinathan, P. Computational and experimental investigation on effective utilization of waste heat from diesel engine exhaust using a fin protracted heat exchanger. *Energy* **2020**, *200*, 117489. [[CrossRef](#)]
6. Kadam, S.T.; Gkouletsos, D.; Hassan, I.; Rahman, M.A.; Kyriakides, A.-S.; Papadopoulos, A.I.; Seferlis, P. Investigation of binary, ternary and quaternary mixtures across solution heat exchanger used in absorption refrigeration and process modifications to improve cycle performance. *Energy* **2020**, *198*, 117254. [[CrossRef](#)]
7. Jung, J.; Jeon, Y.; Cho, W.; Kim, Y. Effects of injection-port angle and internal heat exchanger length in vapor injection heat pumps for electric vehicles. *Energy* **2020**, *193*. [[CrossRef](#)]
8. Wu, J.; Ju, Y. Design and optimization of natural gas liquefaction process using brazed plate heat exchangers based on the modified single mixed refrigerant process. *Energy* **2019**, *186*, 115819. [[CrossRef](#)]
9. Chai, S.; Sun, X.; Zhao, Y.; Dai, Y. Experimental investigation on a fresh air dehumidification system using heat pump with desiccant coated heat exchanger. *Energy* **2019**, *171*, 306–314. [[CrossRef](#)]
10. Toghraie, D.; Mashayekhi, R.; Niknejadi, M.; Arasteh, H. Hydrothermal performance analysis of various surface roughness configurations in trapezoidal microchannels at slip flow regime. *Chin. J. Chem. Eng.* **2020**, *28*, 1522–1532. [[CrossRef](#)]
11. Ghalambaz, M.; Arasteh, H.; Mashayekhi, R.; Keshmiri, A.; Talebizadehsardari, P.; Yaici, W. Investigation of Overlapped Twisted Tapes Inserted in a Double-Pipe Heat Exchanger Using Two-Phase Nanofluid. *Nanomaterials* **2020**, *10*, 1656. [[CrossRef](#)] [[PubMed](#)]
12. Hamid, K.A.; Azmi, W.; Mamat, R.; Sharma, K. Heat transfer performance of TiO₂–SiO₂ nanofluids in a tube with wire coil inserts. *Appl. Therm. Eng.* **2019**, *152*, 275–286. [[CrossRef](#)]
13. Song, X.; Dong, G.; Gao, F.; Diao, X.; Zheng, L.; Zhou, F. A numerical study of parabolic trough receiver with nonuniform heat flux and helical screw-tape inserts. *Energy* **2014**, *77*, 771–782. [[CrossRef](#)]
14. Murugan, M.; Vijayan, R.; Saravanan, A.; Jaisankar, S. Performance enhancement of centrally finned twist inserted solar collector using corrugated booster reflectors. *Energy* **2019**, *168*, 858–869. [[CrossRef](#)]
15. Jaisankar, S.; Radhakrishnan, T.; Sheeba, K. Studies on heat transfer and friction factor characteristics of thermosyphon solar water heating system with helical twisted tapes. *Energy* **2009**, *34*, 1054–1064. [[CrossRef](#)]
16. Ananth, J.; Jaisankar, S. Investigation on heat transfer and friction factor characteristics of thermosyphon solar water heating system with left-right twist regularly spaced with rod and spacer. *Energy* **2014**, *65*, 357–363. [[CrossRef](#)]
17. Saravanan, A.; Senthilkumaar, J.; Jaisankar, S. Experimental studies on heat transfer and friction factor characteristics of twist inserted V-trough thermosyphon solar water heating system. *Energy* **2016**, *112*, 642–654. [[CrossRef](#)]
18. Man, C.; Lv, X.; Hu, J.; Sun, P.; Tang, Y. Experimental study on effect of heat transfer enhancement for single-phase forced convective flow with twisted tape inserts. *Int. J. Heat Mass Transf.* **2017**, *106*, 877–883. [[CrossRef](#)]
19. Lim, K.Y.; Hung, Y.M.; Tan, B.T. Performance evaluation of twisted-tape insert induced swirl flow in a laminar thermally developing heat exchanger. *Appl. Therm. Eng.* **2017**, *121*, 652–661. [[CrossRef](#)]
20. Kumar, N.R.; Bhramara, P.; Kirubeil, A.; Sundar, L.S.; Singh, M.K.; Sousa, A. Effect of twisted tape inserts on heat transfer, friction factor of Fe₃O₄ nanofluids flow in a double pipe U-bend heat exchanger. *Int. Commun. Heat Mass Transf.* **2018**, *95*, 53–62. [[CrossRef](#)]
21. Ho, C.; Chiou, Y.-H.; Yan, W.-M.; Ghalambaz, M. Transient cooling characteristics of Al₂O₃–water nanofluid flow in a microchannel subject to a sudden-pulsed heat flux. *Int. J. Mech. Sci.* **2019**, *151*, 95–105. [[CrossRef](#)]
22. Ghalambaz, M.; Doostani, A.; Izadpanahi, E.; Chamkha, A.J. Conjugate natural convection flow of Ag–MgO/water hybrid nanofluid in a square cavity. *J. Therm. Anal. Calorim.* **2019**, *139*, 2321–2336. [[CrossRef](#)]
23. Mehryan, S.; Ghalambaz, M.; Chamkha, A.J.; Izadi, M. Numerical study on natural convection of Ag–MgO hybrid/water nanofluid inside a porous enclosure: A local thermal non-equilibrium model. *Powder Technol.* **2020**, *367*, 443–455. [[CrossRef](#)]

24. Ho, C.; Liu, Y.-C.; Ghalambaz, M.; Yan, W. Forced convection heat transfer of Nano-Encapsulated Phase Change Material (NEPCM) suspension in a mini-channel heatsink. *Int. J. Heat Mass Transf.* **2020**, *155*. [\[CrossRef\]](#)
25. Ghalambaz, M.; Chamkha, A.J.; Wen, D. Natural convective flow and heat transfer of Nano-Encapsulated Phase Change Materials (NEPCMs) in a cavity. *Int. J. Heat Mass Transf.* **2019**, *138*, 738–749. [\[CrossRef\]](#)
26. Ghalambaz, M.; Groşan, T.; Pop, I. Mixed convection boundary layer flow and heat transfer over a vertical plate embedded in a porous medium filled with a suspension of nano-encapsulated phase change materials. *J. Mol. Liq.* **2019**, *293*. [\[CrossRef\]](#)
27. Chien, L.-H.; Cheng, Y.-T.; Lai, Y.-L.; Yan, W.-M.; Ghalambaz, M. Experimental and numerical study on convective boiling in a staggered array of micro pin-fin microgap. *Int. J. Heat Mass Transf.* **2020**, *149*, 119203. [\[CrossRef\]](#)
28. Chien, L.-H.; Liao, W.-R.; Ghalambaz, M.; Yan, W.-M. Experimental study on convective boiling flow and heat transfer in a microgap enhanced with a staggered arrangement of nucleated micro-pin-fins. *Int. J. Heat Mass Transf.* **2019**, *144*, 118653. [\[CrossRef\]](#)
29. Jaramillo, O.A.; Borunda, M.; Velazquez-Lucho, K.; Robles, M. Parabolic trough solar collector for low enthalpy processes: An analysis of the efficiency enhancement by using twisted tape inserts. *Renew. Energy* **2016**, *93*, 125–141. [\[CrossRef\]](#)
30. Mwesigye, A.; Bello-Ochende, T.; Meyer, J.P. Heat transfer and entropy generation in a parabolic trough receiver with wall-detached twisted tape inserts. *Int. J. Therm. Sci.* **2016**, *99*, 238–257. [\[CrossRef\]](#)
31. Esfe, M.H.; Mazaheri, H.; Mirzaei, S.S.; Kashi, E.; Kazemi, M.; Afrand, M. Effects of twisted tapes on thermal performance of tri-lobed tube: An applicable numerical study. *Appl. Therm. Eng.* **2018**, *144*, 512–521. [\[CrossRef\]](#)
32. Saysroy, A.; Eiamsa-Ard, S. Periodically fully-developed heat and fluid flow behaviors in a turbulent tube flow with square-cut twisted tape inserts. *Appl. Therm. Eng.* **2017**, *112*, 895–910. [\[CrossRef\]](#)
33. Saysroy, A.; Eiamsa-Ard, S. Enhancing convective heat transfer in laminar and turbulent flow regions using multi-channel twisted tape inserts. *Int. J. Therm. Sci.* **2017**, *121*, 55–74. [\[CrossRef\]](#)
34. He, Y.; Liu, L.; Li, P.; Ma, L. Experimental study on heat transfer enhancement characteristics of tube with cross hollow twisted tape inserts. *Appl. Therm. Eng.* **2018**, *131*, 743–749. [\[CrossRef\]](#)
35. Samruaisin, P.; Changcharoen, W.; Thianpong, C.; Chuwattanakul, V.; Pimsarn, M.; Eiamsa-Ard, S. Influence of regularly spaced quadruple twisted tape elements on thermal enhancement characteristics. *Chem. Eng. Process. Process. Intensif.* **2018**, *128*, 114–123. [\[CrossRef\]](#)
36. Ruengpayungsak, K.; Saysroy, A.; Wongcharee, K.; Eiamsa-Ard, S. Thermohydraulic performance evaluation of heat exchangers equipped with centrally perforated twisted tape: Laminar and turbulent flows. *J. Therm. Sci. Technol.* **2019**, *14*, JTST0002. [\[CrossRef\]](#)
37. Hasanpour, A.; Farhadi, M.; Sedighi, K. Intensification of heat exchangers performance by modified and optimized twisted tapes. *Chem. Eng. Process. Process. Intensif.* **2017**, *120*, 276–285. [\[CrossRef\]](#)
38. Hong, Y.; Du, J.; Wang, S. Experimental heat transfer and flow characteristics in a spiral grooved tube with overlapped large/small twin twisted tapes. *Int. J. Heat Mass Transf.* **2017**, *106*, 1178–1190. [\[CrossRef\]](#)
39. Hong, Y.; Du, J.; Wang, S. Turbulent thermal, fluid flow and thermodynamic characteristics in a plain tube fitted with overlapped multiple twisted tapes. *Int. J. Heat Mass Transf.* **2017**, *115*, 551–565. [\[CrossRef\]](#)
40. Eiamsa-Ard, S.; Samravysin, P.; Eiamsa-Ard, S.; Samruaisin, P. Characterization of Heat Transfer by Overlapped-Quadruple Counter Tapes. *J. Heat Transf.* **2018**, *140*, 114501. [\[CrossRef\]](#)
41. Rudrabhiramu, R.; Kumar, K.H.; Rao, K.M. Heat Transfer Enhancement Using Overlapped Dual Twisted Tape Inserts with Nanofluids. In *Advances in Automotive Technologies*; Springer Science and Business Media LLC.: Berlin/Heidelberg, Germany, 2020; pp. 123–130.
42. Qi, C.; Wang, G.; Yan, Y.; Mei, S.; Luo, T. Effect of rotating twisted tape on thermo-hydraulic performances of nanofluids in heat-exchanger systems. *Energy Convers. Manag.* **2018**, *166*, 744–757. [\[CrossRef\]](#)
43. Sundar, L.S.; Singh, M.K.; Punnaiah, V.; Sousa, A.C.M. Experimental investigation of Al₂O₃/water nanofluids on the effectiveness of solar flat-plate collectors with and without twisted tape inserts. *Renew. Energy* **2018**, *119*, 820–833. [\[CrossRef\]](#)
44. Tian, Z.; Abdollahi, A.; Shariati, M.; Amindoust, A.; Arasteh, H.; Karimipour, A.; Goodarzi, M.; Bach, Q.-V. Turbulent flows in a spiral double-pipe heat exchanger. *Int. J. Numer. Methods Heat Fluid Flow* **2019**, *30*, 39–53. [\[CrossRef\]](#)

45. Toghraie, D.; Mashayekhi, R.; Arasteh, H.; Sheykhi, S.; Niknejadi, M.; Chamkha, A.J. Two-phase investigation of water-Al₂O₃ nanofluid in a micro concentric annulus under non-uniform heat flux boundary conditions. *Int. J. Numer. Methods Heat Fluid Flow* **2019**, *30*, 1795–1814. [[CrossRef](#)]
46. Arasteh, H.; Salimpour, M.; Tavakoli, M.R. Optimal distribution of metal foam inserts in a double-pipe heat exchanger. *Int. J. Numer. Methods Heat Fluid Flow* **2019**, *29*, 1322–3142. [[CrossRef](#)]
47. Wei, L.; Arasteh, H.; Abdollahi, A.; Parsian, A.; Taghipour, A.; Mashayekhi, R.; Tlili, I. Locally weighted moving regression: A non-parametric method for modeling nanofluid features of dynamic viscosity. *Phys. A Stat. Mech. Appl.* **2020**, *550*, 124124. [[CrossRef](#)]
48. Rezaei, O.; Akbari, O.A.; Marzban, A.; Toghraie, D.; Pourfattah, F.; Mashayekhi, R. The numerical investigation of heat transfer and pressure drop of turbulent flow in a triangular microchannel. *Phys. E Low Dimens. Syst. Nanostruct.* **2017**, *93*, 179–189. [[CrossRef](#)]
49. Khodabandeh, E.; Toghraie, D.; Chamkha, A.J.; Mashayekhi, R.; Akbari, O.A.; Rozati, S.A. Energy saving with using of elliptic pillows in turbulent flow of two-phase water-silver nanofluid in a spiral heat exchanger. *Int. J. Numer. Methods Heat Fluid Flow* **2019**, *30*, 2025–2049. [[CrossRef](#)]
50. Ghaneifar, M.; Arasteh, H.; Mashayekhi, R.; Rahbari, A.; Mahani, R.B.; Talebizadehsardari, P. Thermohydraulic analysis of hybrid nanofluid in a multilayered copper foam heat sink employing local thermal non-equilibrium condition: Optimization of layers thickness. *Appl. Therm. Eng.* **2020**, *181*, 115961. [[CrossRef](#)]
51. Hong, S.W.; Bergles, A.E. Augmentation of Laminar Flow Heat Transfer in Tubes by Means of Twisted-Tape Inserts. *J. Heat Transf.* **1976**, *98*, 251–256. [[CrossRef](#)]
52. Sarviya, R.; Fuskale, V. Heat Transfer and Pressure Drop in a Circular Tube Fitted with Twisted Tape Insert Having Continuous Cut Edges. *J. Energy Storage* **2018**, *19*, 10–14. [[CrossRef](#)]



© 2020 by the authors. Licensee MDPI, Basel, Switzerland. This article is an open access article distributed under the terms and conditions of the Creative Commons Attribution (CC BY) license (<http://creativecommons.org/licenses/by/4.0/>).